BJRS
BRAZILIAN JOURNAL OF RADIATION SCIENCES

doi.org/10.15392/2319-0612.2025.2895
Braz. J. Radiat. Sci., Rio de Janeiro
2025, 13(3) | 01-26 | e2895
Editor: Prof. Dr. Bernardo Maranhão Dantas
Submitted: 2024-04-14
Accepted: 2025-07-31

In vivo monitoring in radiological or nuclear emergencies: a program for intercomparison of detection efficiency in NaI(Tl) portable detectors

Soares[a*], A. B.; Delgado[a], J. U.; Ferreira Filho[a], Alfredo Lopes; Marques[b], G. F. F.

[a] Radioprotection Dosimetry Institute, 22783-127, Rio de Janeiro, RJ, Brazil.
[b] Army Technology Center, 23031-021, Rio de Janeiro, RJ, Brazil.

Correspondence: *alexandrebaso10@gmail.com

Abstract: In vivo internal monitoring is a laboratory technique used to assess and quantify the incorporation of radionuclides in the human body. Demand for such services may increase significantly in a radiological or nuclear emergency. In addition to dedicated laboratories, researchers have proposed the calibration of portable gamma radiation detectors to carry out a rapid screening of exposed individuals and assess internal dosimetry. Several international intercomparison exercises have been conducted to evaluate the performance of detectors specifically designed for internal monitoring, including, more recently, NaI(Tl) portable detectors. However, these experimental intercomparison exercises have included the transport of radioactive sources between participating institutions. The aim of this study is to propose a simple methodology for determining a reference value for the NaI(Tl) detector efficiency at 662 keV (^{137}Cs), supporting future exercise efforts. This work employed NaI(Tl) scintillator detectors and a torso phantom. It was possible to determine an optimized measurement geometry through simulation using the MCNPX mathematical code, especially regarding the distances, and to estimate efficiency values with defined acceptance intervals for the proposed intercomparison exercise. However, additional experiments are needed to define these intervals more precisely. Complementarily, the minimum detectable effective doses were approximately 60 μSv and 38 μSv for the NaI(Tl) 2”×2” and 3”×1.5” detectors, respectively.

Keywords: internal dosimetry, intercomparison exercises, portable detector efficiencies.

doi.org/10.15392/2319-0612.2025.2895
Braz. J. Radiat. Sci., Rio de Janeiro
2025, 13(3) | 01-26 | e2895
Editor: Prof. Dr. Bernardo Maranhão Dantas
Submitted: 2024-04-14
Accepted: 2025-07-31

Monitoração In Vivo Em Emergência Radiológica: um Programa para Intercomparação da Eficiência de Detecção em Detectores Cintiladores Portáteis

Resumo: A monitoração interna in vivo é uma técnica laboratorial usada para avaliar e quantificar a incorporação de radionuclídeos no corpo humano. A demanda para esse serviço pode aumentar significativamente em casos de emergência radiológica ou nuclear. Além dos laboratórios dedicados, pesquisadores têm proposto a calibração de detectores portáteis de radiação gama para uma rápida monitoração de indivíduos expostos e avaliação da dosimetria interna. Diversos exercícios internacionais de intercomparação têm sido conduzidos para avaliar as respostas de detectores usados em monitoração interna, incluindo, mais recentemente, detectores portáteis de NaI(Tl). Entretanto, esses exercícios experimentais de intercomparação incluem o transporte de fontes radioativas entre as instituições participantes. O objetivo deste estudo é propor uma metodologia simples para a determinação de um valor de referência para a eficiência do detector NaI(Tl), em 662 keV (^{137}Cs), apoiando os esforços para os futuros exercícios. Este trabalhou empregou detectores cintiladores de NaI(Tl) e um simulador de torso. Foi possível determinar uma geometria de medição otimizada por meio de simulação utilizando o código matemático MCNPX, especialmente no que se refere às distâncias, e estimar valores de eficiência com intervalos de aceitação definidos para o exercício de intercomparação proposto.

Palavras-chave: dosimetria interna, exercícios de intercomparação, eficiência de detectores portáteis.

1. INTRODUCTION

In vivo monitoring is an internal dosimetry technique conducted in specialized laboratories. Its purpose is to assess and quantify the incorporation of radionuclides in individuals through ingestion, inhalation, or skin wounds, as well as their deposition in target organs due to physiological [1].

Many countries maintain dedicated internal dosimetry laboratories, specially equipped with gamma-ray spectrometry systems for performing direct measurements on individuals. These detection systems are typically housed in shielded rooms to optimize detection limits, which must be kept as low as possible. In Brazil, five laboratories are part of the Brazilian Network of In Vivo Monitoring Laboratories [2].

In this context, several researchers have recommended the calibration and use of portable detectors, such as solid-state semiconductor (HPGe) and inorganic scintillator NaI(Tl) detectors, for internal dosimetry applications [3–8]. This approach offers an alternative to dedicated internal dosimetry laboratories, particularly in scenarios with potentially high demand, such as radiological or nuclear emergencies.

Each laboratory has established its own methodology for calibrating portable detectors, typically employing commercially available anthropomorphic physical phantoms [9]. These phantoms are prepared with certified radionuclide activities (Bq) and defined measurement geometries, which are sometimes validated through mathematical simulation codes such as the Monte Carlo N-Particle code (MCNPX) [10].

The absolute detection efficiency, ϵ (cps.Bq^{-1}), Minimum Detectable Activity, MDA (Bq), and Minimum Detectable Effective Dose, MDED (μSv), which depends on the Minimum Detectable Intake, MDI (Bq), are key calibration parameters of interest.

The ϵ is defined as the number of pulses recorded divided by the number of radiation quanta emitted by the source [11]. This quantity can be interpreted as the ratio of the count rate to the source activity, weighted by the emission probability of gamma photons at a specific energy (I_γ). The MDA represents the lowest activity value that can be determined, based on the Minimum Detectable Number of Counts (N_D), ϵ, the measurement time Δt, and I_γ [12]. The MDI can be obtained by dividing the MDA by the retention fraction m(t), which is associated with a specific biokinetic model and available in the literature. Then, the MDED can be derived from the product of the MDI and an appropriate dose conversion coefficient [13], [14]. Table 1 summarizes the 662 keV efficiency values published by different authors, based on their respective experimental setups.

Table 1: Detection efficiency (ϵ) values for selected NaI(Tl) detectors as reported in the literature, based on the experimental setups established by the respective authors.

Detector	Phantom	Geometry	ϵ_{abs} at 662 keV (cps.Bq^{-1})	Autor
NaI(Tl) 3"x3"	Thoracic Phantom (PET bottles)[1]	detector at 5 cm of the phantom	2.1 x 10^{-3}	Soares [4]
NaI(Tl) 3"x3"	(lung) IGOR[2]	detector in contact with the chest	(1.5-2.0) x 10^{-3}	Galeev [6]
NaI(Tl) 3"x3"	(whole body) IGOR		(1.0-1.5) x 10^{-3}	
NaI(Tl) 8"x4"	BOMAB[3]	over the torso of the phantom[4]	2.53 x 10^{-3}	Paiva [7]
NaI(Tl) 8"x4"	PET-BOMAB		2.47 x 10^{-3}	
NaI(Tl) 2"x2"	cylindrical plastic bucket (30 x 36 x 0.2 cm^3)	detector in contact with the phantom	5.94 x 10^{-4}	Medici [8]

Notes: 1- PET, polyethylene terephthalate. 2- IGOR, anthropomorphic Phantom. 3- BOMAB, Bottle Manikin Absorber Phantom. 4- the distance data is not available in this reference.

Significant discrepancies in efficiency values are primarily due to differences in the instrumentation and measurement techniques employed, as well as variations in detector crystal volumes, phantom materials and geometries, and source-to-detector distances.

Some international intercomparison exercises have been conducted to evaluate internal dose assessment capabilities, with participation from internal dosimetry laboratories worldwide [15]. The key quantities assessed were the incorporated activity (I) and the

committed effective dose (D_{eff}). However, experimental intercomparison exercises have included the transport of radioactive sources between participating institutions.

The evaluation of the committed effective dose critically depends on the detector counting efficiency. For detectors of the same type (scintillators or semiconductors) and equivalent active volumes, similar efficiency responses are expected under identical measurement conditions. Therefore, establishing a reference counting efficiency value for specific detector types would facilitate intercomparison exercises centered on this parameter.

This study specifically aims to propose a standardized and low-cost methodology for determining reference efficiency values at 662 keV for NaI(Tl) 2”×2” and 3”×1.5” detectors and to estimate the corresponding MDED in a hypothetical scenario involving the inhalation of aerosols containing ^{137}Cs, for the purpose of supporting intercomparison exercises.

2. MATERIALS AND METHODS

Initially, a standardized commercial cylindrical acrylic bucket (30.8 × 35.0 × 0.4) cm^3, which is readily available on the market, was selected to serve as a simple torso phantom by being filled with water to a height of 30 cm. The torso was chosen because it represents a central geometry of the human body and contains many organs of interest in internal dosimetry. Three participants contributed by providing portable inorganic scintillation detectors, consisting of two NaI(Tl) 3”x1.5”, designated #1 and #2, and one NaI(Tl) 2”×2”. These NaI(Tl) 3"×1.5" detectors, manufactured by Mirion Technologies, are robust instruments designed for radionuclide identification in both civilian and military applications. They are equipped with dedicated software for gamma spectrometry (Spectra Management and Identification - SMI) and utilize a 1024-channel multichannel analyzer (MCA). The NaI(Tl) 2”×2” detector, manufactured by Canberra, is a portable device that employs the

Genie2000 software for gamma radiation spectrum analysis and utilizes a 1024-channel multichannel analyzer (MCA).

The radionuclide selected for determining the reference efficiency value was ^{137}Cs, due to its widespread use in various types of calibrations and its availability in numerous nuclear medicine facilities and laboratories. Moreover, ^{137}Cs is a fission product generated in various nuclear reactors and can be released into the environment as aerosols during critical emergencies at nuclear power plants. Consequently, both the public and workers face a risk of internal contamination, primarily through inhalation, underscoring the importance of studying this radionuclide.

The radionuclide ^{137}Cs, after incorporation by inhalation, can be rapidly absorbed from the respiratory tract into the bloodstream and subsequently distributed uniformly throughout the body tissues, where it may remain for an extended period. Like potassium, cesium tends to concentrate in muscle tissues [16]. Therefore, the recommended internal dosimetry approach would be whole-body monitoring in dedicated laboratories [13]. However, since the objective is precisely to use portable detectors, the simplest and most representative geometry for whole-body measurements is torso monitoring.

Moreover, to facilitate the experiments using the torso phantom, a suitable option is the use of a sealed volumetric ^{137}Cs source, whose geometry is widely employed in many metrology laboratories and nuclear medicine services worldwide, eliminating the need for producing new sources.

In this context, it is important to evaluate how similar the detector responses are when comparing the geometries of ^{137}Cs point source distributions inside the torso phantom to that of a ^{137}Cs volumetric source placed at the phantom's geometric center (GC). The possibility of filling the torso phantom with a solution containing ^{137}Cs was not assessed in this study. To carry out this evaluation, the MCNPX mathematical code was employed. Although it is an older version, MCNPX offers several advantages, including

versatility, ease of use, established application in the scientific literature, and availability through one of the study participants.

The MCNPX code, version 2.7a [17], was used to investigate the influence of variations in the geometries of the sealed ^{137}Cs sources placed inside the phantom on the detectors' efficiency responses, particularly with respect to source-to-detector distances. In the input files, the geometries of the sealed sources within the water volume, the active volumes of the detectors, and the source-to-detector distances were simplified and reproduced accordingly. The active volumes of the NaI(Tl) detectors were axially oriented toward the GC in a horizontal direction. The simulated distances from the GC to the face of the active volume ranged from 15.9 cm to 115.4 cm, with variable increments between 0.5 cm and 10 cm. A total of seven source arrangements were considered inside the phantom, as shown in Figure 1, and 140 input files covering 20 different source-to-detector distances were used in the MCNPX code. In all simulation cases, the distance between the point sources was set to 5 cm.

Figure 1: Arrangement of point sources inside the phantom in the MCNPX simulation.

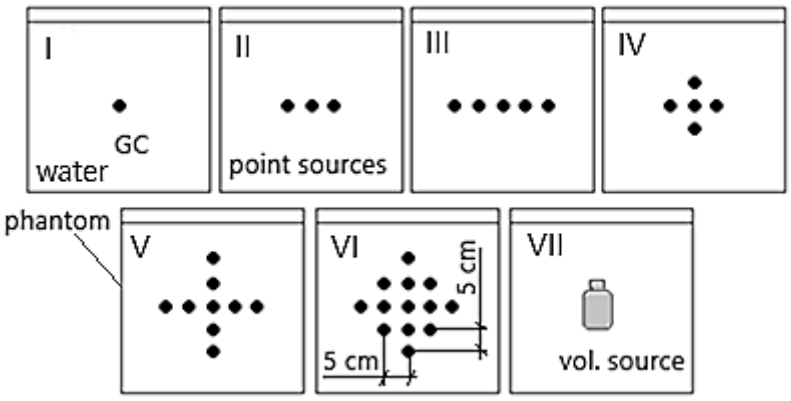

In the mathematical simulations, the following parameters were adopted: a maximum of 10^8 histories; monoenergetic photons with an energy of 662 keV; F8 tally (pulse height distribution in a cell); and E8 energy binning with 1,024 channels spanning the 0–3 MeV range. Regarding the material composition data defined in the input file, the density of

water was set to 0.998207 g/cm³, with weight fraction 0.111894 (H) and 0.888106 (O), and the density of sodium iodide was set to 3.667000 g/cm³, with weight fraction 0.153373 (Na) and 0.846627 (I) [18].

The MCNPX code was executed on a personal computer equipped with an Intel(R) Core (TM) i5-4440 processor (4 cores), a clock speed of 3.10 GHz, and 4 GB of RAM. The simulation time using 10^8 histories ranged from 10 to 16 minutes per input file, with a relative error of 0.0023, well within the reliability threshold (acceptable < 0.10). Detection efficiencies were determined for both detectors based on the count-per-history values, taking into account the different source configurations and the detector-to-phantom distances used in the simulations.

Comparison of the efficiencies obtained for all source arrangements and distances enabled the identification of the distance associated with the lowest percentage standard deviation (SD%), indicating minimal influence from source geometry and positioning within the phantom adopted in this study.

Once the optimized distances were determined through MCNPX simulations, experiments were conducted using volumetric sources. However, in order to also evaluate the detectors' responses to variations in activity levels, sources encapsulated in cylindrical acrylic disks with different available activities were used in specific combinations, since the sealed volumetric sources could not be altered.

Two participants provided sealed radioactive sources with calibration certificates traceable to secondary standards laboratories (Table 2). The types of sealed radioactive sources included volumetric sources of the 20 mL epoxy matrix and point sources, encapsulated at the center of the cylindrical acrylic disk (2 cm x 0.5 cm) (Ø x h) (Figure 2).

Figures 2: Geometry of the sealed radioactive sources: a) volumetric source; b) point source.

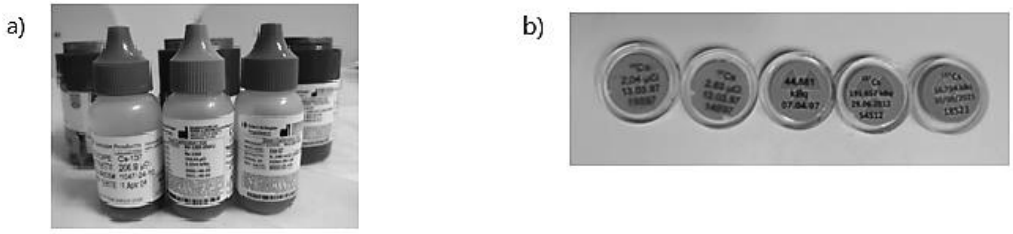

Table 2: Sealed radioactive sources assigned to each detector type as specified.

Source ID #	Radionuclide	Serie number	Activity (Bq)	Reference data	Source Geometry	NaI(Tl) Detector
01	^{57}Co	2262-28-18	1.90 x 10^{8}	01/01/2022	Volumetric	#2
02	^{133}Ba	2090-48-20	9.32 x 10^{6}	01/06/2021	Volumetric	#2
03	^{137}Cs	1047-24-10	7.66 x 10^{6}	01/04/2004	Volumetric	#1, #2
04	^{137}Cs	S8117026-06	3.70 x 10^{6}	11/02/1998	Volumetric	#1
05	^{137}Cs	1111-2-18	7.56 x 10^{6}	01/04/2005	Volumetric	#2 and 2"x2"
06	^{137}Cs	S8117030-02	3.86 x 10^{6}	13/12/1999	Volumetric	#2
07	^{137}Cs	14S97	9.73 x 10^{4}	13/03/1997	Point	#2 and 2"x2"
08	^{137}Cs	37S97	4.49 x 10^{4}	07/04/1997	Point	#2 and 2"x2"
09	^{137}Cs	18S23	1.67 x 10^{4}	30/05/2023	Point	#2 and 2"x2"
10	^{137}Cs	19S97	7.55 x 10^{4}	13/03/1997	Point	#2 and 2"x2"
11	^{137}Cs	54S12	1.92 x 10^{5}	29/06/2012	Point	#2 and 2"x2"
12	^{152}Eu	20S23	5.97 x 10^{4}	11/07/2023	Point	#1 and 2"x2"

The measurements were carried out in the laboratories of two participants who possessed sealed sources. The detector from the third participant, who did not have radioactive sources available, was transported to one of these laboratories.

The sealed sources were encased in a thin plastic film and positioned at the geometric center (GC) of the water volume on a vertical acrylic base. The disk-shaped sources were stacked according to the total activity required for the measurements. Figures 3a and 3b show the measurement setups of the sealed sources and their respective configurations inside the water-filled phantom.

Figure 3. Illustration of the experimental measurement setup: a) volumetric source placed in the phantom with a NaI(Tl) 2"×2" detector; b) stacked point sources placed in the phantom with a NaI(Tl) 3"×1.5" detector.

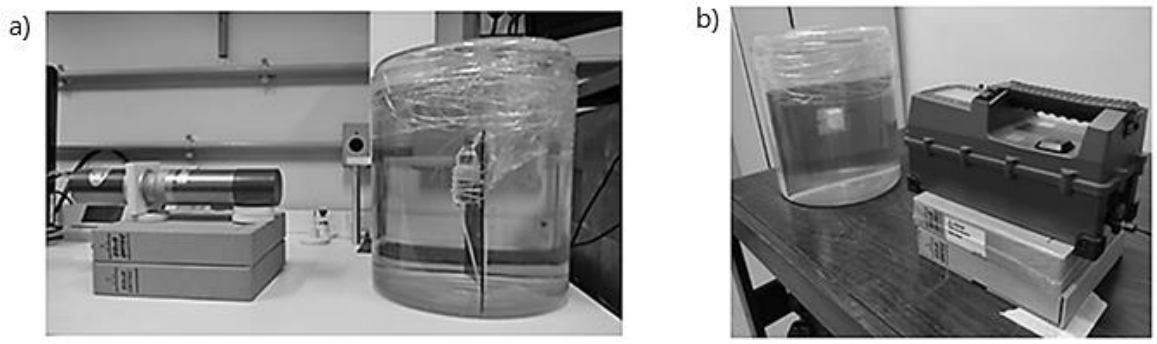

The geometry of the experimental measurements was defined based on the results of the mathematical simulations. The experimental phase began with the acquisition of channel-to-energy calibration curves for each detector, using the available sources: #1 ^{57}Co, #2 ^{133}Ba, and #3 ^{137}Cs for the #2 NaI(Tl) 3"×1.5" detector, and source #12 ^{152}Eu for the other detectors.

Subsequently, the volumetric sealed ^{137}Cs sources (#3 and #4), which were available for measurements with detector #1 NaI(Tl) 3"×1.5", were placed one at a time inside the phantom. Similarly, the sealed ^{137}Cs sources (#3 and #5–11) were designated for measurements with detector #2 NaI(Tl) 3"×1.5", using the same geometry. For the NaI(Tl) 2"×2" detector, sealed sources #5 and #7–11 were designated. The sealed point sources were selected in specific combinations to provide a decreasing gradient in total activity, with the aim of analyzing the influence of activity orders of magnitude on the resulting efficiency values. It is important to highlight that two measurement distances were adopted, one for the NaI(Tl) 2"×2" detector and another for the NaI(Tl) 3"×1.5" detector.

For each source configuration, five measurements were performed for each detector, with a counting time of 1,800 s, forming distinct groups. A total of 9 groups were measured for the NaI(Tl) 2"×2" detector, 7 groups for the #1 NaI(Tl) 3"×1.5" detector, and 10 groups for the #2 NaI(Tl) 3×1.5 detector.

The net count number N_L was obtained by analyzing the gamma radiation spectrum in the Region of Interest (ROI) (662 keV), taking the difference between the total count number (N_T) and the background radiation count number (B). The values of the B counts were determined using equation 1 and the uncertainty of N_L was obtained using equation 2, where B is the count number of the background radiation (BG), from the L channel to the H channel; C_L is the L channel count number; C_H is the count number of the H channel; n is the number of channels in the Region Of Interest (ROI) [19].

$$B = \frac{n(C_L + C_H)}{2} = \frac{(H - L + 1)(C_L + C_H)}{2} \quad \text{Equation 1}$$

$$u = \sigma_{N_L} = \left(\sum_{i=L}^{H} C_i + \frac{n^2(C_L + C_H)}{4} \right)^{1/2} \quad \text{Equation 2}$$

For each of the five measurements in a group, the count rate and the estimate of its propagated uncertainty were calculated using equations 3 and 4, respectively, where R_C is the count rate, N_L is the net count number, Δt is the counting time considered constant (1,800 s), σ_{Rc} is the uncertainty of the count rate, and σ_{NL} is the uncertainty of the net count number.

$$R_C = \frac{N_L}{\Delta t} \quad \text{Equation 3}$$

$$\sigma_{Rc} = \frac{\sigma_{N_L}}{\Delta t} \quad \text{Equation 4}$$

Then, the efficiency was calculated individually for each N_L (equation 5) and its uncertainty was estimated by propagation (equation 6), where ϵ (cps.Bq^{-1}) is the absolute counting efficiency, R_C (s^{-1}) is the counting rate, A (Bq) is the corrected ^{137}Cs activity for the date of the measurements, I_γ is the gamma emission intensity for the 662 keV photopeak of ^{137}Cs (0.852 ±0.001), σ_ϵ is the efficiency uncertainty, σ_{Rc} is the uncertainty of the counting rate, σ_A is the activity uncertainty, and σ_I is the gamma emission intensity uncertainty [11].

$$\epsilon = \frac{R_C}{A \times I_\gamma} \quad \text{Equation 5}$$

$$\frac{\sigma_\epsilon}{\epsilon} = \sqrt{\left(\frac{\sigma_{R_C}}{R_C}\right)^2 + \left(\frac{\sigma_A}{A}\right)^2 + \left(\frac{\sigma_I}{I_\gamma}\right)^2} \qquad \text{Equation 6}$$

In summary, five efficiency values were calculated for each individual measurement within a group, and their weighted mean and associated uncertainty were determined for each group. This procedure enabled the application of the Analysis of Variance (ANOVA) and Tukey statistical tests adopted in this study [20].

For the NaI(Tl) 2"×2" detector, nine groups of five measurements each were conducted, and the corresponding average efficiencies were calculated. These nine mean efficiency values were plotted in graphs to analyze their behavior in relation to the activity levels of the ^{137}Cs sources used in each group. The aim was to identify the activity range suitable for determining a stable average efficiency level. The efficiency value obtained from simulations was also included in these graphs for comparison (Figure 6).

For detectors #1 and #2 NaI(Tl) 3"×1.5", 7 and 10 groups of measurements were performed, respectively, and the results were similarly plotted in graphs illustrating the efficiency–activity relationship (Figures 7 and 8, respectively).

To assess the influence of the activity levels used in the calibrations on the efficiencies obtained, the ANOVA statistical test was applied. ANOVA (Analysis of Variance) is a statistical test used to compare the means of three or more groups and to determine whether at least one of them differs significantly from the others. The test is based on the analysis of the total variability in the data, which is partitioned into two components: between-group variation and within-group variation. If the between-group variation is significantly greater than the within-group variation, the test indicates a statistically significant difference among the group means. The result is expressed as a p-value, with statistical significance typically considered when $p < 0.05$ [20].

In addition, the Tukey test is a statistical procedure applied after ANOVA when a significant difference between groups is detected. Its purpose is to identify which pairs of

means differ significantly from each other. This test compares all possible combinations of groups while controlling for type I errors across multiple comparisons. It calculates a Minimum Significant Difference (MSD) between pairs of means. When the observed difference between two groups exceeds this value, it is considered statistically significant [20].

Subsequently, all measured efficiency values were tested both within each group and across all groups. For the NaI(Tl) 2"×2" detector, all 45 efficiency values (9 groups × 5 measurements) were included; for detectors #1 and #2 NaI(Tl) 3"×1.5", 35 (7 groups × 5 measurements) and 50 (10 groups × 5 measurements) values were tested, respectively.

Thereafter, the Tukey statistical test was applied to identify which activity groups were suitable for calculating the average efficiency to be considered as a reference value for intercomparison, excluding the efficiency values with deviations exceeding the MSD established by the test.

Complementarily, after determining the efficiencies, in order to evaluate the performance of the calibrated systems, measurements were performed on a volunteer at the same calibration distances of the detectors to determine the Minimum Detectable Number of Counts (N_D) and the Minimum Detectable Activity (MDA) for each detector, using equations 7 and 9, where N_{BG} is the count number of the individual, ϵ is the absolute efficiency, Δt is the counting time (600 s), and I_γ is the gamma emission intensity of the 662 keV photopeak of ^{137}Cs (0.852). The uncertainties were estimated according to equations 8 and 10 [11], [12]. The time uncertainties were negligible.

$$N_D = 2.706 + 4.653\sqrt{N_{BG}} = 2.706 + 4.653 \times \sigma_{N_B} \quad \text{Equation 7}$$

$$\sigma_{N_D} = 4.653 \times \frac{1}{2\sqrt{N_{BG}}} \times \sigma_{N_{BG}} = 4.653 \times \frac{1}{2} \cong 2.327 \quad \text{Equation 8}$$

$$MDA = \frac{N_D}{\epsilon \times \Delta t \times I_\gamma} \quad \text{Equation 9}$$

$$\frac{\sigma_{MDA}}{MDA} = \sqrt{\left(\frac{\sigma_{N_D}}{N_D}\right)^2 + \left(\frac{\sigma_\epsilon}{\epsilon}\right)^2 + \left(\frac{\sigma_{I_\gamma}}{I_\gamma}\right)^2} \qquad \text{Equation 10}$$

Considering a scenario of single incorporation by inhalation of ^{137}Cs, the Minimum Detectable Incorporation was obtained by equation 11 [21], where MDI is the minimum detectable incorporation and m(t) is the retention fraction of the radionuclide in the organ or tissue.

$$MDI = \frac{MDA}{m(t)} \qquad \text{Equation 11}$$

Finally, the minimum detectable effective dose (MDED) was calculated for each detector, with the previous data, using equation 10 [13], where e(g) is the dose coefficient for the incorporation conditions.

$$MDED = MDI \times e(g) \qquad \text{Equation 10}$$

The values for m(t) and e(g) are available in the literature (ICRP) according to the type of incorporation and radionuclide [21] and can also be obtained from the AIDE program, an acronym for Activity and Internal Dose Estimates, created to calculate activity in compartments and committed doses due to occupational internal exposures [22].

3. RESULTS AND DISCUSSIONS

The count-per-history number (N_{CTGh}) in the active volume of the detector, obtained from the MCNPX mathematical simulation within the (661.46 to 664.39) keV energy bin, was correlated with the distances between the sealed sources and the detector for each source arrangement inside the phantom (Figure 4). As expected, the detection efficiency is higher at shorter distances and decreases as the distance increases.

The distances at which the differences between the N_{CTGh} values from the seven arrangements were smallest, as determined by the percentage standard deviation calculations

(SD%), were 30.4 cm for the NaI(Tl) 2”×2” detector and 35.4 cm for the NaI(Tl) 3”×1.5” detector (Figure 5). The simulated efficiency results related to these distances were 1.435 × 10^{-4} cps·Bq^{-1} ± 0.83% and 2.245 × 10^{-4} cps·Bq^{-1} ± 0.67% for the NaI(Tl) 2”×2” and 3”×1.5” detectors, respectively.

Figure 4: Detection efficiency behavior as a function of source-to-detector distances. Results obtained from the MCNPX simulation: a) NaI(Tl) 2”x2”; b) NaI(Tl) 3”x1.5”.

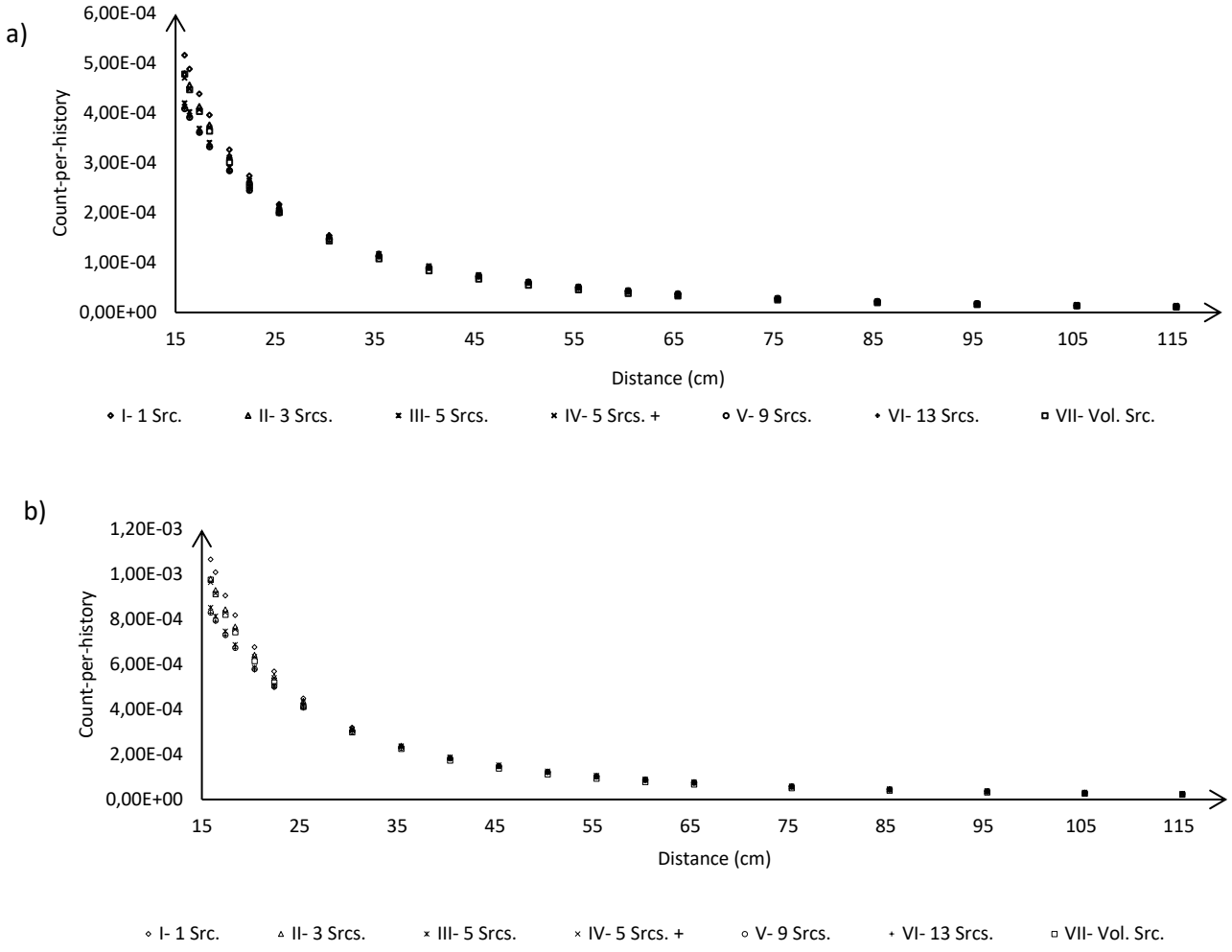

Figure 5: Standard deviations (SD%) of the detector responses for all source arrangements in the phantom, as a function of distance. The curve exhibits a minimum, representing the distance at which the smallest difference between detector responses was observed across all arrangements: a) 2"x2"; b) 3"x1.5".

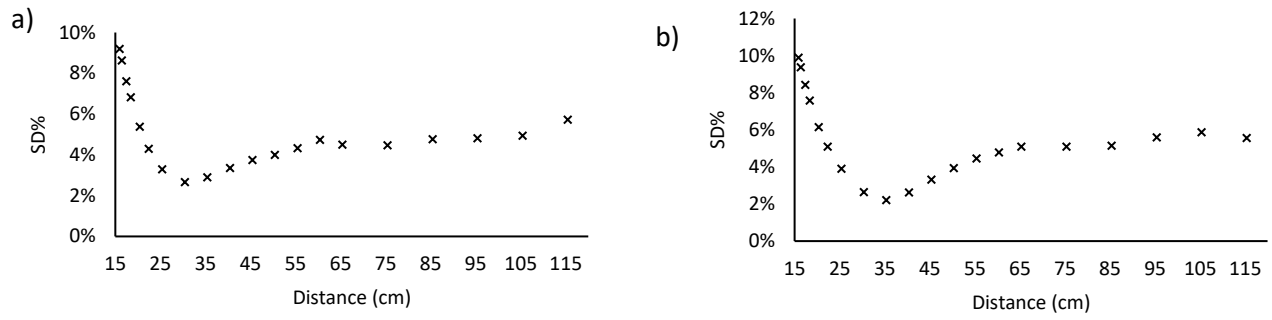

The channel-to-energy calibration curves obtained for the NaI(Tl) 2"×2" and #1 #2 NaI(Tl) 3"×1.5" detectors, demonstrated linearity with an R^2 value equal to 1.

The efficiency values for the 9 groups of the NaI(Tl) 2"×2" detector are presented in Table 3. Significant differences among the group efficiency values were identified through the application of the ANOVA statistical test. The Tukey test analysis indicated that Groups 7 and 9 exhibited the greatest deviations, exceeding the test's Minimum Significant Difference (MSD), and were therefore excluded from further analysis. As a result, the average efficiency of 1.235×10^{-4} cps.Bq^{-1} ± 0.59% was obtained. This value was 13.9% lower than the simulated efficiency value for the volumetric source geometry (1.435×10^{-4} cps·Bq^{-1} ± 0.83%).

Analyzing the efficiency results shown in Figure 6, Groups 6 and 8 were the most critical points still accepted by the Tukey test. Considering the uncertainties of the efficiencies at these points, it can be inferred that a interval of ±10% around the average efficiency value defines a range of values considered acceptable for intercomparison purposes. Therefore, for the purpose of intercomparison, the reference detection efficiency value obtained under the conditions of this study was $(1.235 \pm 0.124) \times 10^{-4}$ cps·Bq^{-1}, corresponding to an uncertainty of 10%.

Table 3: Efficiencies obtained for each group and their respective total activities - NaI(Tl) 2"x2".

Groups	1	2	3	4	5	6	7	8	9
Efficiency ($\times 10^{-4}$) (cps.Bq^{-1})	1.245 ±3.02%	1.265 ±3.02%	1.245 ±3.02%	1.259 ±3.02%	1.246 ±3.02%	1.149 ±3.68%	1.037 ±4.93%	1.179 ±6.92%	1.089 ±9.95%
	1.246 ±3.02%	1.262 ±3.02%	1.237 ±3.02%	1.264 ±3.02%	1.257 ±3.02%	1.157 ±3.68%	0.947 ±5.29%	1.150 ±7.04%	0.866 ±12.59%
	1.237 ±3.02%	1.263 ±3.02%	1.267 ±3.02%	1.261 ±3.02%	1.252 ±3.02%	1.141 ±3.68%	1.045 ±4.91%	1.206 ±6.75%	1.040 ±10.48%
	1.238 ±3.02%	1.261 ±3.02%	1.262 ±3.02%	1.261 ±3.02%	1.244 ±3.02%	1.114 ±3.73%	1.087 ±4.76%	1.120 ±7.20%	1.076 ±10.10%
	1.244 ±3.02%	1.257 ±3.02%	1.270 ±3.02%	1.248 ±3.02%	1.256 ±3.02%	1.140 ±3.68%	1.048 ±4 .90%	1.158 ±7.04%	1.110 ±9.81%
Average ($\times 10^{-4}$) (cps.Bq^{-1})	1.242 ±1.35%	1.262 ±1.35%	1.256 ±1.35%	1.259 ±1.35%	1.251 ±1.35%	1.140 ±1.65%	1.032 ±2.22%	1.162 ±3.12%	1.036 ±4.69%
Sources ID	#5	#5	#5	#5	#5	#7-11	#11	#7-8	#7
Activity ($\times 10^{6}$ Bq)	4,87	4,87	4,87	4,87	4,87	0,27	0,14	0,07	0,05

Figure 6: Simulated, experimental, and average efficiencies, along with the defined acceptance interval. The graph shows the behavior of experimental efficiency as a function of activity for the NaI(Tl) 2"×2" detector.

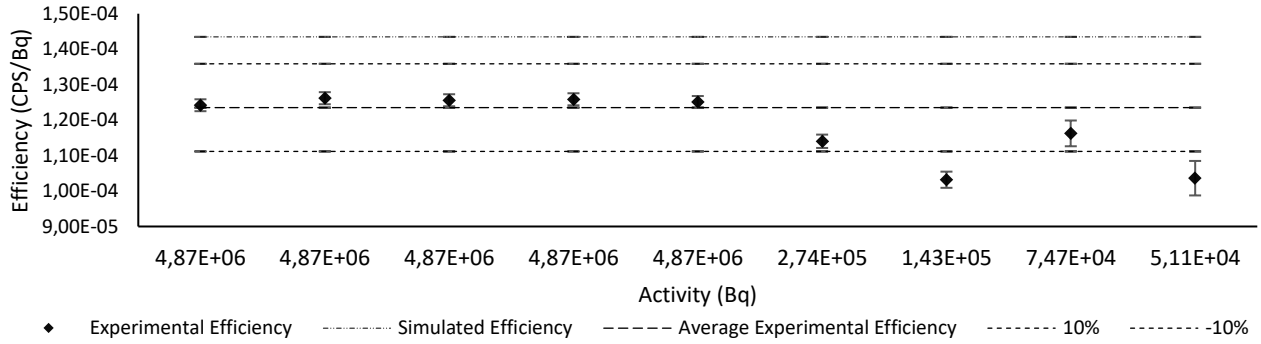

Similarly, the efficiency values for the 7 groups of the #1 NaI(Tl) 3"×1.5" detector are presented in Table 4. Significant differences among the group efficiency values were identified through the application of the ANOVA statistical test. The Tukey test analysis indicated that Groups 3, 5 and 7 exhibited the greatest deviations, exceeding the test's Minimum Significant Difference (MSD), and were therefore excluded from further analysis. As a result, the average efficiency of 1.826×10^{-4} cps.Bq^{-1} ± 0.68% was obtained. This value was 18.7% lower than the simulated efficiency value for the volumetric source geometry (2.245×10^{-4} cps·Bq^{-1} ± 0.67%).

Analyzing the efficiency results shown in Figure 7, Group 1 was the most critical point still accepted by the Tukey test. Considering the uncertainty of efficiency at this point, it can be inferred that a margin of ±4.5% around the average efficiency value defines a range of values considered acceptable for intercomparison purposes. Therefore, for intercomparison purposes, the reference experimental efficiency value obtained under the conditions of this study was $(1.826 \pm 0.082) \times 10^{-4}$ cps·Bq^{-1}, corresponding to a relative uncertainty of 4.5%.

Table 4: Efficiencies obtained for each group and their respective total activities - #1 3"x1.5".

Groups	1	2	3	4	5	6	7
Efficiency (x 10^{-4}) (cps.Bq^{-1})	1.871 ±3.03%	1.807 ±3.03%	1.749 ±3.03%	1.755 ±3.03%	1,589 ±3.07%	1.810 ±3.06%	1.723 ±3.06%
	1.869 ±3.03%	1.811 ±3.03%	1.755 ±3.03%	1.795 ±3.03%	1.603 ±3.07%	1.826 ±3.06%	1.717 ±3.07%
	1.879 ±3.03%	1.807 ±3.03%	1.768 ±3.03%	1.806 ±3.03%	1.569 ±3.08%	1.851 ±3.06%	1.712 ±3.07%
	1.873 ±3.03%	1.810 ±3.03%	1.760 ±3.03%	1.798 ±3.03%	1.558 ±3.08%	1.847 ±3.06%	1.728 ±3.07%
	1.901 ±3.02%	1.812 ±3.03%	1.773 ±3.03%	1.789 ±3.03%	1.560 ±3.08%	1.831 ±3.06%	1.719 ±3.07%
Average (x 10^{-4}) (cps.Bq^{-1})	1.878 ±1.35%	1.809 ±1.35%	1.761 ±1.35%	1.788 ±1.35%	1.576 ±1.38%	1.833 ±1.37%	1.720 ±1.37%
Sources ID	#3	#3	#3	#3	#4	#4	#4
Activity (x 10^6 Bq)	4.84	4.83	4.83	4.82	2.03	2.03	2.02

Figure 7: Simulated, experimental, and average efficiencies, along with the defined acceptance interval. The graph shows the behavior of experimental efficiency as a function of activity for the #1 NaI(Tl) 3"×1,5" detector.

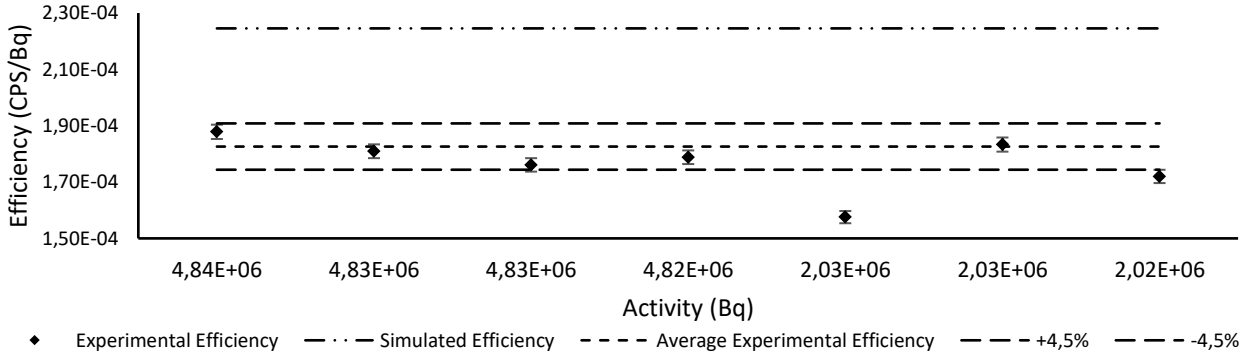

Lastly, the efficiency values for the 10 groups of the #2 NaI(Tl) 3"×1.5" detector are presented in Table 5. Significant differences among the group efficiency values were identified through the application of the ANOVA statistical test. The Tukey test analysis indicated that Groups 9 and 10 exhibited the greatest deviations, exceeding the test's Minimum Significant Difference (MSD), and were therefore excluded from further analysis. As a result, the average efficiency of 1.878×10^{-4} cps.Bq^{-1} ± 0.51% was obtained. This value was 16.4% lower than the simulated efficiency value for the volumetric source geometry (2.245×10^{-4} cps·Bq^{-1} ± 0.67%).

Analyzing the efficiency results shown in Figure 8, Groups 1 and 8 were the most critical points still accepted by the Tukey test. Considering the uncertainty of efficiency at this point, it can be inferred that a margin of ±14% around the average efficiency value defines a range of values considered acceptable for intercomparison purposes. Therefore, for intercomparison purposes, the experimental efficiency value obtained under the conditions of this study was $(1.878 \pm 0.263) \times 10^{-4}$ cps·Bq^{-1}, corresponding to a relative uncertainty of 14%.

Table 5: Efficiencies obtained for each group and their total respective activities - #2 3"x1.5".

Groups	1	2	3	4	5	6	7	8	9	10
Efficiency (x 10^{-4}) (cps.Bq^{-1})	1.982 ±3.01%	1.869 ±3.02%	1.877 ±3.02%	1.881 ±3.02%	1.878 ±3.02%	1.879 ±3.02%	1.882 ±3.59%	1.615 ±4.81%	1.184 ±10.51%	0.707 ±30.21%
	1.982 ±3.01%	1.860 ±3.02%	1.865 ±3.02%	1.870 ±3.02%	1.889 ±3.02%	1.889 ±3.02%	1.890 ±3.58%	1.628 ±4.80%	1.299 ±9.53%	0.300 ±72.25%
	1.988 ±3.01%	1.873 ±3.02%	1.877 ±3.02%	1.891 ±3.02%	1.891 ±3.02%	1.873 ±3.02%	1.905 ±3.57%	1.651 ±4.75%	1.206 ±10.23%	0.566 ±37.82%
	1.984 ±3.01%	1.865 ±3.02%	1.884 ±3.02%	1.869 ±3.02%	1.887 ±3.02%	1.886 ±3.02%	1.923 ±3.56%	1.652 ±4.74%	1.128 ±11.00%	0.517 ±41.41%
	1.994 ±3.01%	1.872 ±3.02%	1.873 ±3.02%	1.878 ±3.02%	1.887 ±3.02%	1.888 ±3.02%	1.921 ±3.56%	1.729 ±4.58%	1.155 ±10.73%	0.462 ±46.61%
Average (x 10^{-4}) (cps.Bq^{-1})	1.986 ±1.35%	1.868 ±1.35%	1.875 ±1.35%	1.878 ±1.35%	1.886 ±1.35%	1.883 ±1.35%	1.904 ±1.60%	1.654 ±2.12%	1.195 ±4.64%	0.510 ±18.77%
Sources ID	#6-5	#3	#3	#3	#3	#3	#7-11	#11	#7-8	#10
Activity (x 10^6 Bq)	6.98	4.79	4.79	4.79	4.79	4.79	0.27	0.14	0.07	0.04

Figure 8: Simulated, experimental, and average efficiencies, along with the defined acceptance interval. The graph shows the behavior of experimental efficiency as a function of activity for the #2 NaI(Tl) 3"×1,5" detector.

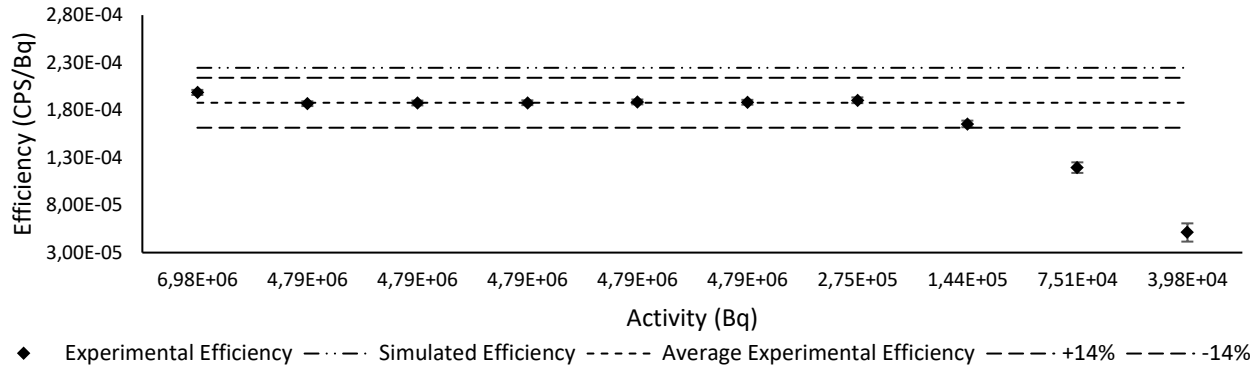

The percentage difference between the experimental efficiency values obtained for the 3"×1.5" detectors (1.826 × 10^{-4} and 1.878 × 10^{-4} cps.Bq^{-1}) was 2.7%, indicating good agreement between these results. The average of these values was 1.852 × 10^{-4} cps·Bq^{-1}, which is 17.5% lower than the simulated value. On the other hand, the difference between the experimental and simulated efficiencies for the 2"×2" detector (1.235 × 10^{-4} and 1.435 × 10^{-4} cps·Bq^{-1}, respectively) was -13.9%. This last experimental value was similar to that found by Medici (5.94 × 10^{-4} cps·Bq^{-1}), showing consistency even with the differences in source-to-detector distances.

These discrepancies between the experimental and simulated values are likely due to the simplified geometry adopted for the detectors in the MCNPX code, which did not account for the presence of several attenuating materials surrounding the active volumes, such as aluminum, as well as the fact that the simulated results were extracted from histograms.

The #1 and #2 NaI(Tl) 3"×1.5" detectors average efficiency (1.852 × 10^{-4} cps·Bq^{-1}), when compared to the efficiency of the NaI(Tl) 2"×2" detector (1.235 × 10^{-4} cps.Bq^{-1}), the resulting ratio is 1.50. The ratio between the active volumes of these detectors (102.96 cm^3 and 173.75 cm^3) is 1.68. Therefore, the experimental efficiency values were considered consistent with the respective active volumes of the detectors, as higher efficiencies are expected to be proportional to the detectors' active volumes.

Despite the agreement between the experimental efficiency values for detectors #1 and #2 NaI(Tl) 3×1.5, it is important to note that the intervals values, ±4.5% and ±14.0%, respectively, around the mean efficiency, derived from the Tukey statistical test analysis, were notably discrepant. This finding suggests the need to reproduce the methodology with a larger number of detectors in future studies.

Although the activities used in this study were limited by the availability of sources, it was observed that the efficiencies tended to show greater deviations from the mean under conditions involving the lowest activity values used in the experiments (Figures 7 at 9). This is a relevant point in the present context, given that the ratio between the count rate measured by the detector and the activity may not follow a linear relationship outside a certain activity range, either at higher orders of magnitude due to dead-time effects, or at lower levels due to poor counting statistics. This issue requires further investigation in future studies, as it may compromise intercomparison exercises focused on efficiency as the primary quantity.

Complementarily, the Minimum Detectable Effective Dose (MDED) was calculated using the efficiency of each detector, obtained under the calibration conditions established in this study, the volunteer's background radiation count measurements, the counting time (600 s), a retention fraction m(t) of 7.610×10^{-1} Bq/Bq, and a dose coefficient e(g) of 5.60×10^{-6} mSv/Bq. The calculation considered an Activity Median Aerodynamic Diameter (AMAD) of 5 μm and moderate absorption (type M) in the lungs [21]. The results are presented in Table 6.

Table 6: Results for the Minimum Detectable Effective Dose.

NaI(Tl)	N_{BG}	Time (s)	N_D	Effic. x10^{-4} (CPS.Bq^{-1})	MDA (Bq)	m(t)	MDI (Bq)	e(g) x10^{-6} mSv/Bq	MDED (μSv)
2"x2"	12003 ±0.91%	600	512 ±0.45%	1.235 ±0.59%	8187 ±0.75%	0.7610	10760 ±0.75%	5.60	60.2 ±0.75%
#1 3"x1.5"	10885 ±0.96%	600	488 ±0.48%	1.826 ±0.68%	5226 ±0.84%		6868 ±0.84%		38.5 ±0.84%

NaI(Tl)	N_{BG}	Time (s)	N_D	Effic. x10^{-4} (CPS.Bq^{-1})	MDA (Bq)	m(t)	MDI (Bq)	e(g) x10^{-6} mSv/Bq	MDED (µSv)
#2 3"x1.5"	10386 0.98%	600	477 ±0.49%	1.878 ±0.51%	4997 ±0.71%		6567 ±0.71%		36.8 ±0.71%

It is important to highlight that it is common practice in many organizations to recommend internal monitoring for workers who operate under normal occupational exposure conditions or in accident scenarios, in cases where the likelihood of radionuclide intake over one year may result in an effective dose exceeding 1 mSv [13].

Although the primary aim of this study is the intercomparison of detector efficiencies under standardized calibration conditions, that is, all participants should be able to reproduce the proposed experimental methodology, the results demonstrate that the system can exhibit sufficient sensitivity to comply with internal monitoring recommendations, particularly in scenarios involving ^{137}Cs aerosol inhalation, depending on the background radiation level at the measurement site.

This finding highlights the potential applicability of the proposed methodology beyond efficiency assessment, supporting its use in practical internal dosimetry, while acknowledging the limitations of the phantom in terms of its similarity to a real human torso and the representation of ^{137}Cs deposition in the lungs during the initial moments following intake.

4. CONCLUSIONS

According to the objective of the present study, it was possible to define a simple and easily reproducible methodology, using a commercially standardized and low-cost cylindrical acrylic bucket to serve as a torso phantom, along with certified sealed sources. Based on the analysis of the MCNPX simulation results, the source-to-detector distances defined for the intercomparison exercises were 30.4 cm and 35.4 cm for the 2"×2" and 3"×1.5" NaI(Tl) detectors, respectively. New distances will need to be determined for other active volumes of NaI(Tl) detectors. It was possible to estimate the efficiency values and their respective intervals for intercomparison purposes. However, additional experiments are needed to more accurately define these intervals. Complementarily, the minimum detectable effective doses were approximately 60 μSv and 38 μSv for the NaI(Tl) 2”×2” and 3”×1.5” detectors, respectively, using the setup established in this study for a hypothetical scenario of ^{137}Cs aerosol inhalation. These results indicate their potential applicability in internal dosimetry, depending on comparisons with the results obtained from the application of more realistic phantom models available in the literature. Finally, it is expected that this methodology will be reproduced for other NaI(Tl) scintillation detectors in order to expand the statistical dataset and establish reference efficiency values for use in intercomparison exercises.

ACKNOWLEDGMENT

We thank our colleagues from Centro Tecnológico do Exército (CTEx) and Hospital de Força Aérea do Galeão (HFAG) who provided portable detectors.

CONFLICT OF INTEREST

The authors declare that there is no conflict of interest in the production of this work.

REFERENCES

[1] INTERNATIONAL ATOMIC ENERGY AGENCY (IAEA). Assessment of Occupational Exposure Due to Intakes of Radionuclides. IAEA Safety Standards Series. No. RS-G-1.2, IAEA, Vienna, 1999.

[2] DANTAS, B. M., LUCENA, E. A., CARDOSO, J. S., LIMA, F. L., MENDES, B. M., RAMOS, M. P., DANTAS, A. L. A. *In*: BRAZILIAN CONGRESS ON IONIZING RADIATION METROLOGY 2019, Florianópolis, Brazil. **Brazilian Network of In Vivo Monitoring Laboratories: Current situation and future prospects**. Florianópolis: CBMRI, 2019.

[3] CICIANI, L.; VILARDI, I.; RIZZO, A.; ANTONACCI, G.; BATTISTI, P.; CASTELLANI, C. M.; SPERANDIO, L.. In vivo public monitoring in emergency exposure scenarios. **The European Physical Journal Plus**, Italy, v. 136, p. 1-15, 2021.

[4] SOARES, A. B.; LUCENA, E. A.; DANTAS, A. A.; ARBACH, M. N.; DANTAS, B. M.. Development and calibration of a portable detection device for in vivo measurement of high-energy photon emitters incorporated by humans. **Brazilian Journal of Radiation Sciences**, Brazil, v. 6, n. 2A (Suppl.), 2018.

[5] YOSHITOMI, H.; NISHINO S.; TANIMURA, Y.; TAKAHASHI, M.. A study of a calibration technique for a newly developed thyroid monitor and its uncertainties due to body size for radioiodine measurements. **Radiation Measurements**, Japan, v. 133, p. 106279, 2020.

[6] GALEEV, R.; BUTTERWECK, G.; BOSCHUNG, M.; HOFSTETTER-BOILLAT, B.; HOFFMANN, E.; MAYER, S.. Suitability of Portable Radionuclide Identifiers for Emergency Incorporation Monitoring. **Radiation Protection Dosimetry**, v. 173, n. 1-3, p. 145-150, 2017.

[7] PAIVA, F. G.; MENDES, B. M.; SILVA, T. A.; LACERDA, M.A.S; PINTO, J.R.; PRATES, S.; FILHO N.N.A.; DANTAS, A.L.A.; DANTAS, B.M.; FONSECA, T.C.F.. Calibration of the LDI/CDTN Whole Body Counter Using Three Physical Phantoms. **Brazilian Journal of Radiation Sciences**, Brazil, v. 5, n. 3, 2017.

[8] MEDICI, S.; CARBONEZ, P.; DAMET, J.; BOCHUD, F.; PITZSCHKE, A.. Use of portable gamma spectrometers for triage monitoring following the intake of conventional and novel radionuclides. **Radiation Measurements**, v. 136, p. 106426, 2020.

[9] BOCHUD, F.; LAEDERMANN, J. P.; BAECHLER, S.; BAILAT, C.; BOSCHUNG, M.; AROUA, A.; MAYER, S.. Monte Carlo Simulation of a whole-Body Counter Using Igor Phantoms. **Radiation Protection Dosimetry**, v. 162, n. 3, p. 280-288, 2014.

[10] ALMISNED, GHADA; M. H. ZAKALY, HESHAM; T. ALI., FATEMA; A. M. ISSA, SHAMS; ENE A, ANTOANETA; KILIC, GOKHAN; IVANOV, V.; TEKIN, H. O.. A closer look at the efficiency calibration of LaBr3 (Ce) and NaI (Tl) scintillation detectors using MCNPX for various types of nuclear investigations. **Heliyon**, v. 8, n. 10, 2022.

[11] KNOLL, G. F.. Counting Statistics and Error Prediction. **Radiation Detection and Measurement**. Michigan: John Wiley & Sons, Inc, 2000. p. 86-96. ISBN 0-471-07338-5.

[12] CURRIER, LLOYD A.. Limits for Qualitative Detection and Quantitative Determination: Application to radiochemistry. **Analytical Chemistry Division**. National Bureau of Standards, v.40, n.3, p. 586-593, 1968.

[13] INTERNATIONAL COMMISSION ON RADIOLOGICAL PROTECTION (ICRP). Occupational Intakes of Radionuclides: Part 1. Publication nº 130, Oxford, 2015.

[14] INTERNATIONAL COMMISSION ON RADIOLOGICAL PROTECTION (ICRP). Occupational Intakes of Radionuclides: Part 3. Publication nº 137, Oxford, 2015.

[15] CASTELLANI, C. M.; ANDRÁSI, A.; GIUSSANI, A.; PÁZMÁNDI, T.; ROBERTS, G.. Preliminary Results of the Icidose 2017 International Intercomparison on Internal Dose Assessment. **Radiation Protection Dosimetry**, v.136, n. 4, p. 535-541, 2019.

[16] ARGONNE NATIONAL LABORATORY. Radiological and Chemical Fact Sheets to Support Health Risk Analyses for Contaminated Areas. U.S. Department of Energy (DOE), Illinois, 2007.

[17] WATERS, L. S. (2002). MCNPX User's Manual Version 2.3.0. Los Alamos National Laboratory Los Alamos, New Mexico, 2002.

[18] MCCONN, R. J.; GESH, C.J.; PAGH, R.T.; RUCKER, R.A.; WILLIAMS, R.G. III. Radiation Portal Monitor Project: Compendium of Material Composition Data for Radiation Transport Modeling (PNNL-15870 Rev. 1). Pacific Northwest National Laboratory, 2011.

[19] INTERNATIONAL STANDARD (ISO). Measurement of radioactivity — Gamma ray emitting radionuclides — Generic test method using gamma-ray spectrometry. British Standard, ISO 20042:2019(E), Geneva, 2019.

[20] MONTGOMERY, D. C. **Design and Analysis of Experiments**. 9th edition. John Wiley & Sons, Inc., 2017. ISBN 9781119113478.

[21] INTERNATIONAL ATOMIC ENERGY AGENCY (IAEA). Assessment of Occupational Exposure Due to Intakes of Radionuclides. VIENNA: v. No. RS-G-1.2, 1999.

[22] BERTELLI, L; MELO, D. R.; LIPSZTEIN, J.; CRUZ-SUAREZ R.. AIDE: Internal Dosimetry Software. **Radiation Protection Dosimetry**, Oxford, v. 130, n. 3, p. 358-367, 2008.

LICENSE